Signal and Backward Raman Pump Power Optimization in Multi-Band Systems Using Reliable and Fast Power Profile Estimation

Y. Jiang, J. Sarkis, S. Piciaccia, F. Forghieri, and P. Poggiolini

***Abstract*—This paper presents an efficient numerical method for calculating spatial power profiles of both signal and pump with significant Interchannel Stimulated Raman Scattering and backward Raman amplification in multiband systems. This method was tested in the optimization of a C+L+S/C+L+S+E 1000 km link, employing three backward Raman pumps, by means of a closed-form EGN model (CFM6). The results show a 100x computational speed increase, enabling deep optimization which made it possible to obtain very good overall system performance and flat GSNR.**

***Index Terms*—CFM, CFM6, closed-form model, ISRS, multiband, power-profile calculation, Raman amplification.**

I. Introduction

MULTIBAND systems have emerged as a solution to enhance the capacity of optical communication networks. The extension from the traditional C-band to C+L has been successfully implemented in commercial systems, effectively doubling system throughput. Ongoing research is focused on incorporating additional bands, such as S, U, and even E and O [1], [2], [3], [4], [5].

In multiband systems, Interchannel Stimulated Raman Scattering (ISRS) is very strong. Among the techniques that have been explored to mitigate the impact of ISRS, launch power spectrum optimization and selective Backward Raman amplification have been shown to be quite effective [1]. However, such techniques are typically based on iterative algorithms and, to be practical, they need to be supported by very fast physical layer models. The traditional numerically-integrated GN [6] and EGN models [7] are too slow, by several orders of magnitude. Closed-form models (CFMs) are needed.

Received 27 February 2025; revised 16 June 2025; accepted 27 June 2025. Date of publication 3 July 2025; date of current version 2 September 2025. This work was supported in part by Cisco Systems through the BOOST Research Contract and in part by the PhotoNext Center of Politecnico di Torino, and in part by European Union through Italian National Recovery and Resilience Plan (NRRP) of NextGenerationEU, partnership on "Telecommunications of the Future" (PE00000001 - Program "RESTART"). *(Corresponding author: Y. Jiang.)*

Y. Jiang, J. Sarkis, and P. Poggiolini are with the Dipartimento di Elettronica e Telecomunicazioni (DET), Politecnico di Torino, 10129 Torino, Italy (e-mail: yanchao.jiang@polito.it).

S. Piciaccia and F. Forghieri are with the CISCO Photonics, 20871 Vimercate (MB), Italy.

Color versions of one or more figures in this article are available at https://doi.org/10.1109/JLT.2025.3585684.

Digital Object Identifier 10.1109/JLT.2025.3585684

Two research groups, one at University College London (UCL), and one at Politecnico di Torino (PoliTo) in collaboration with CISCO, have independently developed over the last few years fast Non-Linear Interference (NLI) CFMs, based on the GN and EGN physical layer models. For the UCL CFM see [8], [9], for the CISCO-PoliTo CFM see [10], [11].

These CFMs are highly effective, to the extent that they are no longer the primary computational overhead. Instead, the dominant factor has become Spatial Power Profile (SPP) estimation. The CFMs need the SPP of each channel along each span to produce accurate NLI estimation.

The computation of the SPPs is typically based on numerically solving the coupled differential Raman equations, which account for both ISRS and Raman amplification [12]. Conventional numerical methods, such as MATLAB ODE solvers, handle such computation efficiently when ISRS alone is present. However, when *backward* Raman amplification is introduced, the problem transforms into a dual-boundary-condition one, which is much slower to resolve. SPP estimation, such as the bvp4c algorithm in MATLAB, then becomes the dominant computational bottleneck, consuming 95% or more of the total time required to evaluate overall system throughput.

Several approaches have been proposed to expedite SPP calculations. Some rely on approximations, such as assuming a triangular-shaped Raman gain spectrum. While fast, this method is affected by substantial error. Other approaches try to speed up computation by modifying the integration algorithm. For instance, [13] finds a coarse SPP solution by assuming frequency-independent pump depletion, and then takes such solution as a starting point to find the actual one. However, the speed-up achieved with this method is relatively modest.

Another method [14] focuses exclusively on *backward* propagation, projecting the forward direction onto the backward. It employs vectorization techniques to enhance computational efficiency. However, while this method is very fast when it converges, it has frequent convergence failures which lead to unreliable performance, limiting its practical applicability.

Nonetheless, we found [14] very promising and in this paper we developed a similar algorithm that both further improved computational efficiency and solved the convergence issues. Similar to [14], propagation is unidirectional. Differently from it, we focus exclusively on *forward* propagation. Rather than computing effective length and Raman gain as intermediate steps,

we operate directly on SPP calculation. To ensure numerical stability, we also developed techniques to prevent divergence. Eventually, we got approximately a 200x speed increase vs. conventional bvp4c algorithms, while consistently ensuring convergence.

As test case-studies for the algorithm, we looked at long-haul SMF systems operating in the C+L+S (CLS for short) and C+L+S+E (CLSE for short) bands, with backward Raman amplification. Both the WDM launch power spectrum and backward Raman amplification are optimized, first to maximize throughput and then also to ensure Generalized Signal-to-Noise Ratio (GSNR) flatness. Thanks to the deep optimization made possible by the CFM and the sped-up SPP estimation algorithm, we obtain excellent overall system performance, combining high throughput with flat GSNR.

This paper is a follow-up to [15]. With respect to [15] we have revised and improved the algorithm, greatly expanded on its description and completely recalculated all results after adding double Rayleigh back-scattering (DRB), which is a non-negligible contribution to noise when backward Raman amplification is significant. We have explicitly reported the objective functions used for optimization and discussed the different weights that can be used for achieving different levels of GSNR flatness. CLS results are new, as well as CLSE with GSNR flatness. Only CLSE for maximum throughput was already in [15], but without DRB. We have also added full EGN-model checks of the final CFM-based results.

This paper is organized as follows. In Section II the fast power profile algorithm is introduced. In Section III the system is described in detail and GSNR results are reported and extensively discussed. Comments and conclusion follow.

II. The Reliable and Fast SPP Algorithm

The SPP along a span of a channel or a backward Raman pump (BRP) can be found using the well-known coupled Raman differential equations. In the following, please keep in mind that we call 'lightwaves' both the individual transmission channels and the individual BRPs. We identify each lightwave through an index n associated to its center frequency f_n. Note that both transmission channels and BRPs can actually act as 'pumps', that is they can feed power to another lightwave, or as 'probes', that is they can receive power from another lightwave.

Systems can also make use of forward Raman Pumps (FRPs), though this is a niche technique used on rare occasions. In the following we will not mention them explicitly. If present, FRPs are treated by the algorithm exactly as the forward-propagating transmission channels.

For the n-th lightwave, its power profile $P_n(z)$ is given by:

$$\pm\frac{dP_n(z)}{dz} = -2\cdot\alpha_n\cdot P_n(z) + \left\{\sum_{j=1}^{N}\varsigma\left(f_n,f_j\right)\cdot C_R(f_n,f_j)\cdot P_j(z)\right\}\cdot P_n(z) \tag{1}$$

where the upper sign in the left is used when $P_n(z)$ is a forward-propagating lightwave, the lower sign is used when it is a counter-propagating lightwave. Note that in practical systems the counter-propagating lightwaves consist of just BRPs, whereas the forward-propagating lightwaves consist of channels and possibly FRPs as well. Such equations can be re-written in integral form:

$$P_n(z) = P_n(0)\cdot\exp\left\{\mp 2\cdot\alpha_n\cdot z \pm\sum_{j=1}^{N}\varsigma\left(f_n,f_j\right)\cdot C_R(f_n,f_j)\cdot\int_0^z P_j(\xi)\,d\xi\right\} \tag{2}$$

where N is the total number of lightwaves, α_n represents the intrinsic fiber loss at the frequency f_n and $C_R(f_n,f_j)$ represents the gain/loss coefficient experienced by the n-th lightwave due to the presence of the j-th lightwave. The function $\varsigma(f_n,f_j)$ is (f_n/f_j) when $f_n > f_j$, 1 when $f_n < f_j$ and 0 when $f_n = f_j$.

The system of N coupled equations (2) is a double-boundary value problem, which typically needs many forward-backward iterations to achieve a solution starting from a reasonable guess. One alternative is [14] which, though iterative as well, only resorts to *backward* solutions, that can be put into a very computationally efficient matrix form, dealing with all the coupled equations at once. We tried this approach but, as mentioned in Section I, we found substantial convergence problems.

We decided therefore to focus instead on *forward*-only propagation and directly on SPPs to iteratively find the final solution. We also used a matrix form to speed up computations. Calling $\mathbf{P}$ the matrix whose rows are the spatial samples of the n-th lightwave SPP, taken at $z = m\cdot\Delta z$ along the span in the forward direction, that is, $\mathbf{P} = [P_n(m\cdot\Delta z)]_{N\times M}$, $m = 0,1,2,\ldots,M$, $M = \frac{L_{\text{span}}}{\Delta z}$, Δz is the step size, L_{span} is the span length. We can generate the $(k+1)$-th power-profile iteration from the k-th as follows:

$$\mathbf{P}^{(k+1)} = \mathbf{P}_{\text{in}}^{(k)}\cdot\exp\left\{\mp 2\cdot\boldsymbol{\alpha}\cdot\mathbf{z}\pm\Delta z\cdot\mathbf{C}_R\cdot\mathbf{P}^{(k)}\cdot\mathbf{U}\right\} \tag{3}$$

where:

$$\mathbf{P}_{\text{in}}^{(k)} = \text{diag}\left(\left(P_n^{(k)}(0)\right)_{N\times N}\right)$$

$$\boldsymbol{\alpha} = (\alpha_n)_{N\times 1}\,,\quad \mathbf{z} = (m\cdot\Delta z)_{1\times M}$$

$$\mathbf{C}_R = [\varsigma\left(f_n,f_j\right)\cdot C_R(f_n,f_j)]_{N\times N}$$

$$\mathbf{U} = \begin{bmatrix} 0 & \frac{1}{2} & \frac{1}{2} & \frac{1}{2} & \ldots & \frac{1}{2}\\ 0 & \frac{1}{2} & 1 & 1 & \ldots & 1\\ 0 & 0 & \frac{1}{2} & 1 & \ldots & 1\\ 0 & 0 & 0 & \frac{1}{2} & \ldots & 1\\ \vdots & \vdots & \vdots & \vdots & \ddots & \vdots\\ 0 & 0 & 0 & 0 & \ldots & \frac{1}{2}\end{bmatrix}_{M\times M} \tag{4}$$

Note that the product $(\Delta z\cdot\mathbf{P}\cdot\mathbf{U})$ in (3) performs numerical integration according to the trapezoidal method, in the forward direction. Note also that even the BRPs are fictitiously propagated forward by (3). This is mathematically possible by flipping

the sign of the intrinsic loss α_n and Raman gain C_R in (2) and (3) for all lightwaves that physically back-propagate, but are dealt with by the algorithm as forward-propagating.

At the first iteration, (3) needs to be initialized with a guess of the SPPs for all lightwaves, across the entire span: $\mathbf{P}^{(0)}$. This matrix also directly implies the boundary condition at ($z = 0$), that is $\mathbf{P}^{(0)}_{\text{in}}$. The initialization of $\mathbf{P}^{(0)}$ is a critical aspect of the algorithm and will be discussed later in Section II-A.

Once $\mathbf{P}^{(0)}$ has been initialized, then (3) generates the next iteration, $\mathbf{P}^{(1)}$, which in turn generates $\mathbf{P}^{(2)}$, and so on. Ideally, the algorithm has converged when *both* $\mathbf{P}^{(k+1)} = \mathbf{P}^{(k)}$ *and* the power of each BRP at $z = L_{\text{span}}$ coincides with its nominal launch power value.

After substantial testing, we found that this algorithm had better reliability, but still convergence failed occasionally. Also, there were limitations as to the pump power that it was capable to handle. Therefore, we improved the algorithm by devising suitable strategies to both assign the initial condition $\mathbf{P}^{(0)}$ and to adapt the SPPs fed to (3) at *each successive iteration*. The goal was to ensure that each iteration generated a solution $\mathbf{P}^{(k)}$ closer to the accurate result, while avoiding divergence, oscillations, or excessive iterations.

A. Initialization

Here we show the algorithm in detail, by means of pseudo-code in Algorithm 1. If no modification is imposed on the BRPs, the initial SPPs are calculated based on the nominal launch powers of all lightwaves and the intrinsic fiber loss, similar to [14], which generates $[\mathbf{P}^{(0)}_{\text{signal}}; \tilde{\mathbf{P}}^{(0)}_{\text{pump}}]$. When using these SPPs as $\mathbf{P}^{(0)}$, the algorithm would diverge due to the significant power transfer from BRPs to signals at the fiber end in all the case-studies in Section III.

We therefore propose scaling BRPs by a factor of $t_{s,\text{dB}}$ so that the two total launch powers of BRPs and the transmission channels coincide, if the total BRPs launch powers at $z = L_{\text{span}}$ is larger than that of the transmission channels at $z = 0$. Otherwise, they are left unchanged. This yields a good initial SPPs $\mathbf{P}^{(0)} = [\mathbf{P}^{(0)}_{\text{signal}}; \mathbf{P}^{(0)}_{\text{pump}}]$.

However, the goal of the algorithm is to find a solution where the boundary conditions on launch powers are satisfied both at $z = 0$ for the transmission channels and at $z = L_{\text{span}}$ for the BRPs. We pre-define a series of power references $P^{(k)}_{\text{pump,ref}}$ at $z = L_{\text{span}}$ to gradually scale BRPs from initial powers up to the launch powers by small steps. Smaller steps $\delta^{(k)}_{\text{dB}}$ are taken when the difference between nominal BRP launch powers and the ones after the k-th iteration is smaller. Generally, we can set 0.2 dB at the first iteration, decreasing linearly to 0 dB at the last iteration. This way, we can define the number of iterations L_{iter} to make $\sum_{k=1}^{k=L_{\text{iter}}} \delta^{(k)}_{\text{dB}} = t_{s,\text{dB}}$, $\delta^{(k)}_{\text{dB}} > \delta^{(k+1)}_{\text{dB}}$.

Notably, $\delta^{(k)}_{\text{dB}}$ simultaneously define BRPs powers reference $P^{(k)}_{\text{pump,ref}}$ for each iteration. As the forward-nature of the algorithm does not impose any constraint on the SPP values at $z = L_{\text{span}}$, we need to rescale BRPs SPPs to $P^{(k)}_{\text{pump,ref}}$ in each iteration. The k-th BRPs reference is,

$$P^{(k)}_{\text{pump,ref}} = P^{(k-1)}_{\text{pump,ref}} + \delta^{(k)}_{\text{dB}}$$

with the starting values of $P^{(0)}_{\text{pump,ref}} = \mathbf{P}^{(0)}_{\text{pump}}(L_{\text{span}})$.

Algorithm 1: SPPs Calculator.

INITIALIZATION:
(1) $\mathbf{P}^{(0)} = [\mathbf{P}^{(0)}_{\text{signal}}; \mathbf{P}^{(0)}_{\text{pump}}]$
SPPs are calculated based only on fiber loss
BRPs SPPs are scaled down by a factor of $t_{s,\text{dB}}$
to coincide the total launch power with that of the
forward-propagating lightwaves
(2) L_{iter}: number of iterations
(3) $\delta^{(k)}_{\text{dB}}$: the k-th step for generating $P^{(k)}_{\text{pump,ref}} while$
linearly decreasing along the iterations
START SPPs calculation:
While $k <= L_{\text{iter}}$ **do**
1. run forward (3):
$\tilde{\mathbf{P}}^{(k)} = [\mathbf{P}^{(k)}_{\text{signal}}; \tilde{\mathbf{P}}^{(k)}_{\text{pump}}]$
If NaN appears in SPPs **then**
Diverge, and move to the conventional method
end if
2. prepare the k-th BRPs reference $\mathbf{P}^{(k)}_{\text{pump,ref}}$:
$P^{(k)}_{\text{pump,ref}} = P^{(k-1)}_{\text{pump,ref}} + \delta^{(k)}_{\text{dB}}$
3. rescale $\tilde{\mathbf{P}}^{(k)}_{\text{pump}}$ w.r.t. $\mathbf{P}^{(k)}_{\text{pump,ref}}$:
$\mathbf{P}^{(k)}_{\text{pump}} = \tilde{\mathbf{P}}^{(k)}_{\text{pump}} / \tilde{\mathbf{P}}^{(k)}_{\text{pump,out}} \cdot \mathbf{P}^{(k)}_{\text{pump,ref}}$
4. update $\mathbf{P}^{(k)}$:
$\mathbf{P}^{(k)} = [\mathbf{P}^{(k)}_{\text{signal}}; \mathbf{P}^{(k)}_{\text{pump}}]$
end while

B. Iterative SPPs Calculator

After the initialization, loading $\mathbf{P}^{(0)}$ into (3) generates $\tilde{\mathbf{P}}^{(1)} = [\mathbf{P}^{(1)}_{\text{signal}}; \tilde{\mathbf{P}}^{(1)}_{\text{pump}}]$ in the forward direction. The solution $\tilde{\mathbf{P}}^{(1)}$ in general contains values of the BRPs at $z = L_{\text{span}}$ that are different from $P^{(1)}_{\text{pump,ref}}$, as addressed in Section II-A.

Before re-inserting $\tilde{\mathbf{P}}^{(1)}$ into (3), BRPs SPPs are modified to match $P^{(1)}_{\text{pump,ref}}$ at $z = L_{\text{span}}$. This creates $\mathbf{P}^{(1)}$, that is passed into (3), producing $\tilde{\mathbf{P}}^{(2)}$. Again, the BRP SPPs are scaled up/down slightly according to the same law and a new matrix $\mathbf{P}^{(2)}$ is obtained and passed through (3) to obtain $\tilde{\mathbf{P}}^{(3)}$, and so on.

As the iterations keep going, the gap between the BRP launch power in the fiber at the algorithm k-th step $\tilde{\mathbf{P}}^{(k)}$ is gradually reduced versus the *nominal* BRP launch power. The algorithm stops when all BRPs launch powers are back to their nominal values and no significant fluctuations are detected in the transmission channels SPPs.

Using this feedback-guided scaling strategy, we have been able to obtain very reliable convergence for the algorithm, which we have tested in very high pump and channel power situations, well beyond practical levels, with excellent results. Despite

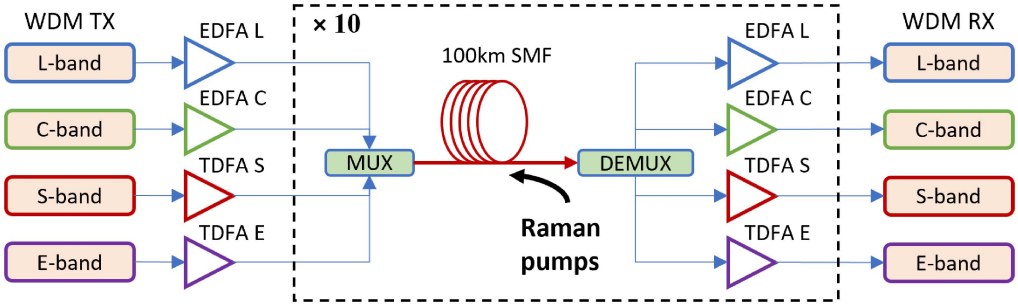

Fig. 1. Schematic of the 10-span CLSE system being studied. Fiber parameters are slightly different among spans (see text).

the algorithm requiring typically 50 to 200 iterations, due to its efficient matrix formulation and inherent features, it has consistently proved about 200x faster than our Matlab reference algorithm (bvp4c) in SPPs calculation only.

We will come back on performance testing in Section III-D.

III. System Case Studies

We tested the sped-up algorithm on the optimization of a CLS and a CLSE 10-span system, with BRPs in the higher-frequency bands. The use of BRPs has proven quite beneficial for such multiband links.

These systems require complex launch power optimization, as well as Raman pump (power and frequency) optimization. In turn, this entails hundreds or thousands of full-system evaluations, which would be very difficult to carry out without a CFM and, due to the presence of BRPs, without an efficient SPP calculation algorithm. They are therefore ideal for testing the proposed SPP calculation algorithm.

Incidentally, while using this as a case-study for testing the SPP algorithm, we obtain interesting system results that have their own validity and impact. We will comment on the resulting system indications at the bottom of the paper. However, these should be viewed as test-cases and not a systematic system study, which is left for future investigation.

A. System Description

The schematic is shown in Fig. 1. The first five spans, all slightly different from one another, were characterized from the experimental set-up used for CFM validation in [17]. Loss and dispersion were measured in C and L band and then extrapolated to the S and E band (Fig. 2(a)) using well-known formulas [18]. The Raman gain spectrum $C_R(f, f_p)$ was experimentally characterized using a pump at $f_p = 206.5$ THz (the green curve in Fig. 2(b)). It was shifted and scaled as a function of f and f_p, according to [19]. The black line in Fig. 2(b) shows the Self-Phase Modulation (SPM) coefficient γ vs. frequency.

The first five spans were then extrapolated to 100 km each and replicated, to achieve a total system length of 1000 km. The insertion loss from the MUX/DEMUX and all other connectors was assumed to be 4 dB at the end of each span. The average total span loss was 22 dB at 193 THz.

The WDM band boundaries set here were: L-band 184.50 to 190.35; C-band 190.75 to 196.60; S-band 197.00 to 202.85;

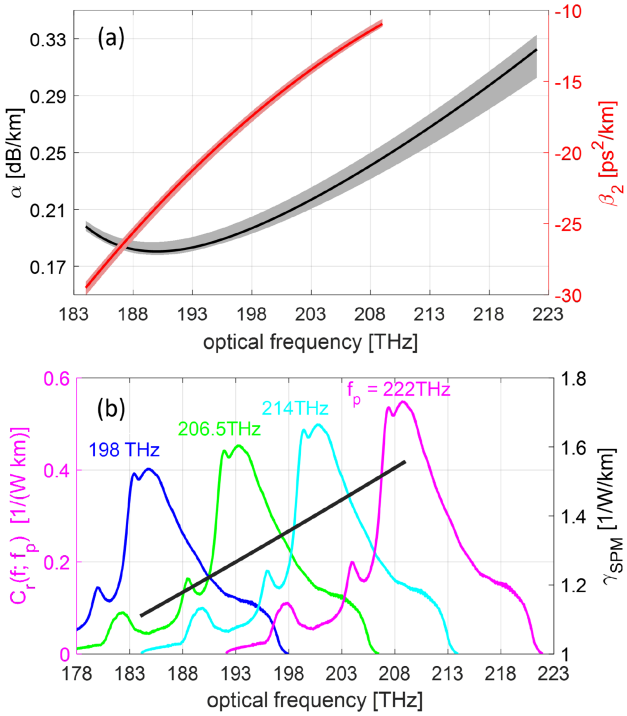

Fig. 2. (a) Loss and dispersion, measured in C and L bands and extrapolated to S and E bands. The solid curve represents the mean value, while the shaded area indicates the range. (b) Raman Gain spectrum and SPM coefficient γ.

E-band 203.25 to 209.07 THz. Doped-Fiber-Amplifiers (DFAs) were assumed, with a noise figure of 5 dB in the C-band, 6 dB in the L and S-bands, and 7 dB in the E-band. Each band contained 50 equally-spaced channels, with a symbol rate of 100 GBaud, roll-off 0.1, and spacing of 118.75 GHz. The modulation was taken to be Gaussian-shaped. The *net* per-channel throughput of the transceivers, vs. GSNR at the receiver input, was assumed as shown in Fig. 3. While not specific to any part number of any vendor, Fig. 3 is loosely representative of the performance expected of top-of-the-line transceivers using probabilistic shaping, operating at about 100 GBaud. BRPs were included, consisting of three pumps.

B. Launch Power and GSNR

Specifically, the launch power spectrum in each band and the frequency and power of the three BRPs were optimized first

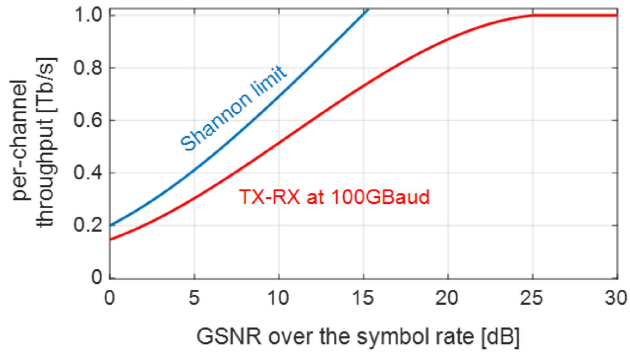

Fig. 3. Transceiver net per-channel throughput vs. GSNR.

for *maximum throughput*, and then GSNR ((6)) flatness. Note that the launch power spectrum was described using a cubic polynomial in each band:

$$P_{\mathrm{ch,dB}}(f) = a_0 + a_1(f - f_c) + a_2(f - f_c)^2 + a_3(f - f_c)^3 \tag{5}$$

with f_c being the center frequency of each band. This spectrum representation requires a total of 12 coefficients for CLS and 16 coefficients for CLSE systems (4 per band) and significantly simplifies the optimization problem as compared to a per-channel power optimization. The launch power spectrum is assumed to be the same at the start of each span, assuming the presence of programmable optical filters (POF) in DFAs, as it is commonplace in latest-generation units.

The system GSNR at the receiver is defined as:

$$\mathrm{GSNR} = \frac{P_{\mathrm{ch}}}{P_{\mathrm{ASE}} + P_{\mathrm{NLI}} + P_{\mathrm{DRB}}} \tag{6}$$

where P_{ch} is the power of the channel being tested and P_{ASE}, P_{NLI}, P_{DRB} are the power of ASE noise, of NLI noise, and of DRB noise [20], respectively, at the receiver.

All three types of noise power at the receiver can be calculated as:

$$P_{\mathrm{X}} = \sum_{n_{\mathrm{s}}=1}^{N_{\mathrm{s}}} P_{\mathrm{X}}^{(n_{\mathrm{s}})} \cdot \Gamma(n_{\mathrm{s}}+1, N_{\mathrm{s}}), \mathrm{X} \in \{\mathrm{ASE, NLI, DRB}\} \tag{7}$$

where $\Gamma(n_{\mathrm{s}}+1, N_{\mathrm{s}})$ represents the linear propagation of the noise from the $(n_{\mathrm{s}}+1)$-th span to the receiver (totally N_{s} spans), after it is generated at the n_{s}-th span. It is assumed that the span loss of each channel is fully and exactly compensated for at the end of the span, taking ISRS into account. Therefore, $\Gamma(n_{\mathrm{s}}+1, N_{\mathrm{s}}) = 1$. Otherwise, the linear propagation factor must be taken into account. We now concentrate on the noise generated at the n_{s}-th span.

1) ASE Noise: P_{ASE} contains ASE noise from both DFAs ($P_{\mathrm{ASE,DFA}}$) and BRPs ($P_{\mathrm{ASE,RA}}$). At the n_{s}-th span, ASE noise power is calculated by:

$$\begin{aligned} P_{\mathrm{ASE}}^{(n_{\mathrm{s}})} &= P_{\mathrm{ASE,DFA}}^{(n_{\mathrm{s}})} \cdot G_{\mathrm{POF}}^{(n_{\mathrm{s}})} + P_{\mathrm{ASE,RA}}^{(n_{\mathrm{s}})} \cdot G_{\mathrm{end}}^{(n_{\mathrm{s}})} \\ P_{\mathrm{ASE,DFA}}^{(n_{\mathrm{s}})} &= h \cdot f_n \cdot (G_{\mathrm{DFA}}^{(n_{\mathrm{s}})} - 1) \cdot F_{\mathrm{DFA}} \cdot B \end{aligned} \tag{8}$$

where $G_{\mathrm{POF}}^{(n_{\mathrm{s}})}$ is the loss provided by POF. $G_{\mathrm{end}}^{(n_{\mathrm{s}})}$ is the gain/loss provided by the components (MUX/DEMUX, DFAs, POF and other connectors) between the n_{s}-th and $(n_{\mathrm{s}}+1)$-th spans to ensure the same launch power across all spans. $G_{\mathrm{DFA}}^{(n_{\mathrm{s}})}$ is the gain provided by DFAs, which is assumed to be flat and equal to the maximum gain required to compensate for the span loss in each band. h is Planck constant. F_{DFA} is the noise figure of DFAs. B is the bandwidth of each channel centered at f_n. The calculation of $P_{\mathrm{ASE,RA}}^{(n_{\mathrm{s}})}$ is based on the differential equation [21]:

$$\begin{aligned} \frac{P_{n,\mathrm{ASE,RA}}^{(n_{\mathrm{s}})}(z)}{dz} =& -2 \cdot \alpha_n \cdot P_{n,\mathrm{ASE,RA}}^{(n_{\mathrm{s}})}(z) \\ &+ \left\{ \sum_{j=1}^{N} \varsigma(f_n, f_j) \cdot C_R(f_n, f_j) \cdot P_j(z) \right\} \\ &\cdot \left(P_{n,\mathrm{ASE,RA}}^{(n_{\mathrm{s}})}(z) + 2 \cdot h \cdot f_n \cdot B \cdot F_{jn} \right) \\ F_{jn} =& \begin{cases} N_{\mathrm{phon}} + 1, f_j > f_n \\ -N_{\mathrm{phon}}, f_j < f_n \end{cases} \\ N_{\mathrm{phon}} =& \frac{1}{1 - \exp\left(-\frac{h \cdot |f_j - f_n|}{k_B \cdot T}\right)} \end{aligned} \tag{9}$$

where k_B is Boltzmann constant. T is the temperature of the system. The initial value at the start of each span is 0.

2) NLI Noise: The NLI noise is calculated using CFM6 [11]. The Machine learning factors are taken from Table IV in [22]. Specifically, the expression of NLI power generated at the n_{s}-th span is (2) in [11].

3) DRB Noise: $P_{\mathrm{DRB}}^{(n_{\mathrm{s}})}$ is expressed as,

$$\begin{aligned} P_{\mathrm{DRB}}^{(n_{\mathrm{s}})} =& G_{\mathrm{end}}^{(n_{\mathrm{s}})} \cdot P_{\mathrm{ch}} \cdot G_{0,L_{\mathrm{span}}} \cdot \kappa^2 \\ & \int_0^L \int_0^{z_1} G_{z_1 z_2}^2 dz_2 dz_1 \end{aligned} \tag{10}$$

where κ is Rayleigh back-scattering coefficient, assumed to be -40 dB/km across all channels, $G_{z_1 z_2}$ is the gain/loss from z_1 to z_2.

C. System Optimization and Result

The system was then optimized. Each BRP is constrained to be at least 2 THz away from the signals and is limited to 1 W, while no constraints are imposed on the signal powers. In Fig. 4(a) we show the CLS system results, with throughput maximization. The objective function is:

$$f_{\mathrm{obj}} = \mathrm{mean}\left(\mathrm{T}_{\mathrm{Rx}}^n\right) \tag{11}$$

where $\mathrm{T}_{\mathrm{Rx}}^n$ is the net throughput of the n-th channel, obtained from the GSNR through the red curve in Fig. 3. The optimum launch power per channel is represented by the dashed black curve, with average power of -0.3 dBm, 0 dBm and 3.6 dBm in the L, C and S band, respectively. The S band requires significantly higher power to compensate for the greater loss caused by higher nominal fiber attenuation and ISRS, even with

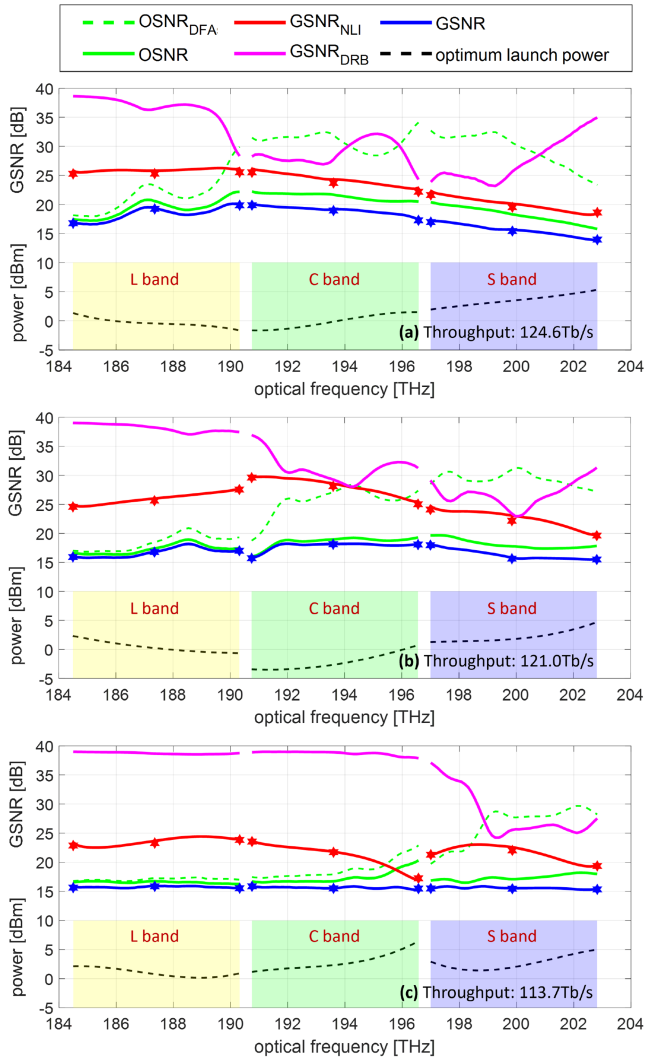

Fig. 4. CLS optimum launch power per channel and GSNRs for (a) throughput maximization using (11); (b) throughput maximization while flattening GSNR using (12) with $w = 0.5$; (c) throughput maximization while flattening GSNR using (12) with $w = 1$.

TABLE I
PUMP CONFIGURATIONS

System	Case	Pump 1		Pump 2		Pump 3	
		Freq [THz]	Power [dBm]	Freq [THz]	Power [dBm]	Freq [THz]	Power [dBm]
CLS (Fig. 4)	(a)	205.1	21.5	211.5	27.7	214.0	26.6
	(b)	206.7	21.3	212.4	26.6	214.8	26.8
	(c)	212.4	22.2	214.0	25.2	217.0	25.5
CLSE (Fig. 7)	(a)	212.4	22.6	217.5	25.7	220.6	28.7
	(b)	213.1	22.2	217.8	25.7	220.8	28.9
	(c)	214.0	17.4	219.2	24.0	221.7	27.9

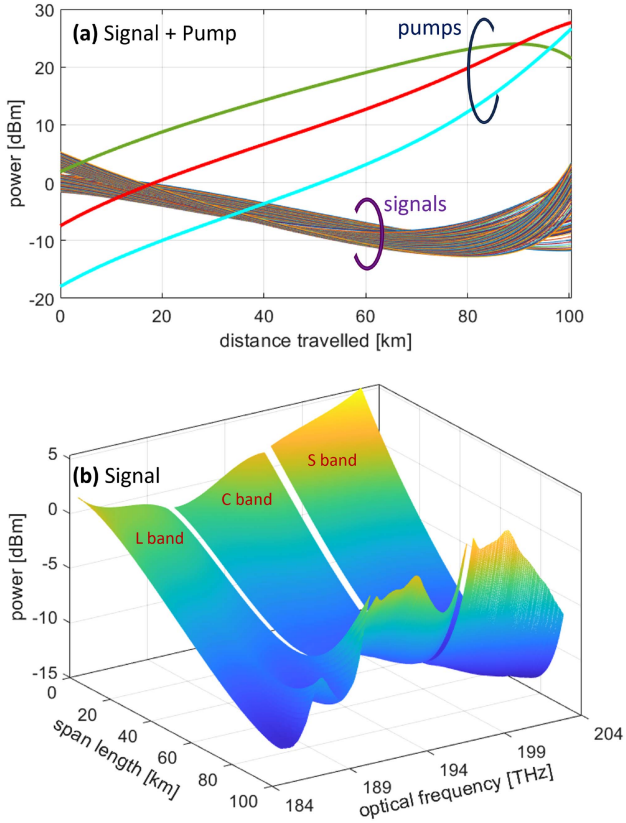

Fig. 5. SPPs in the first span (a) 2D plot of all lightwaves; (b) 3D plot of all signals in the CLS system of Fig. 4(a).

the backward Raman amplification. The optimized BRPs are listed in Table I.

Fig. 4(a) displays total GSNR as well as various partial signal-to-noise ratios: OSNR (ASE only, DFAs+Raman), GSNR_{NLI} (NLI only), GSNR_{DRB} (DRB only). OSNR_{DFA} accounts for ASE from DFAs but not from BRPs. The much higher value of OSNR_{DFA} in the C and S bands, as compared to OSNR, means that most amplification was delivered by BRPs in those bands. This can also be seen from the SPP plots in Fig. 5. The channels in both C band S bands experienced high gain from BRPs. This introduced more DRB noise in these two bands. Fig. 6(a) displays the Raman on-off gain using blue curves presenting the span in Fig. 5, demonstrating that DRB noise should be considered when the Raman on-off gain exceeds 20 dB. All spans exhibit similar behavior. Also, notice that all C and S channels are technically in nonlinear regime, that is, with $\text{GSNR}_{\text{NLI}} - OSNR < 3\,\text{dB}$ [23].

Next, GSNR flatness was incorporated into the objective function to reduce GSNR variations, while still maximizing throughput. The objective function is modified as:

$$f_{\text{obj}} = \text{mean}\left(\text{T}_{\text{Rx}}^{n}\right) - w* \mid \text{T}_{\text{Rx}}^{\max} - \text{T}_{\text{Rx}}^{\min} \mid \qquad (12)$$

where w is a weight used for controlling the flatness of GSNR. A bigger w induces a flatter GSNR. $\text{T}_{\text{Rx}}^{\max}$ and $\text{T}_{\text{Rx}}^{\min}$ are the maximum and minimum values of T_{Rx}^{n}, respectively.

Fig. 4(b) shows the results with $w = 0.5$. The optimum launch power per channel is represented by the dashed black curve, with average power of 0.5 dBm, −2 dBm and 0.5 dBm in the L, C and S band, respectively. The optimized BRPs are listed in Table I. The peak-to-peak GSNR variation was reduced to 2.7 dB from 6.2 dB, while the throughput went marginally down to 121.0 b/s

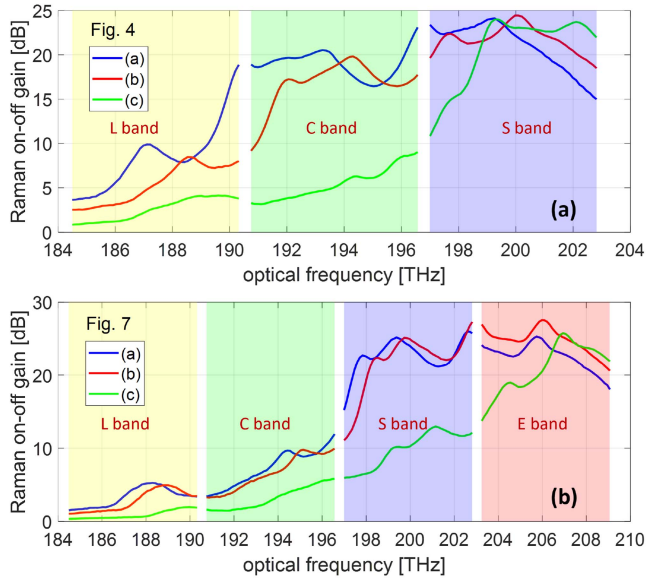

Fig. 6. Raman on-off gain in the first span of (a) CLS system; (b) CLSE system. The blue, red and green curves represent the scenarios (a), (b) and (c), respectively, as shown in Fig. 4 and Fig. 7.

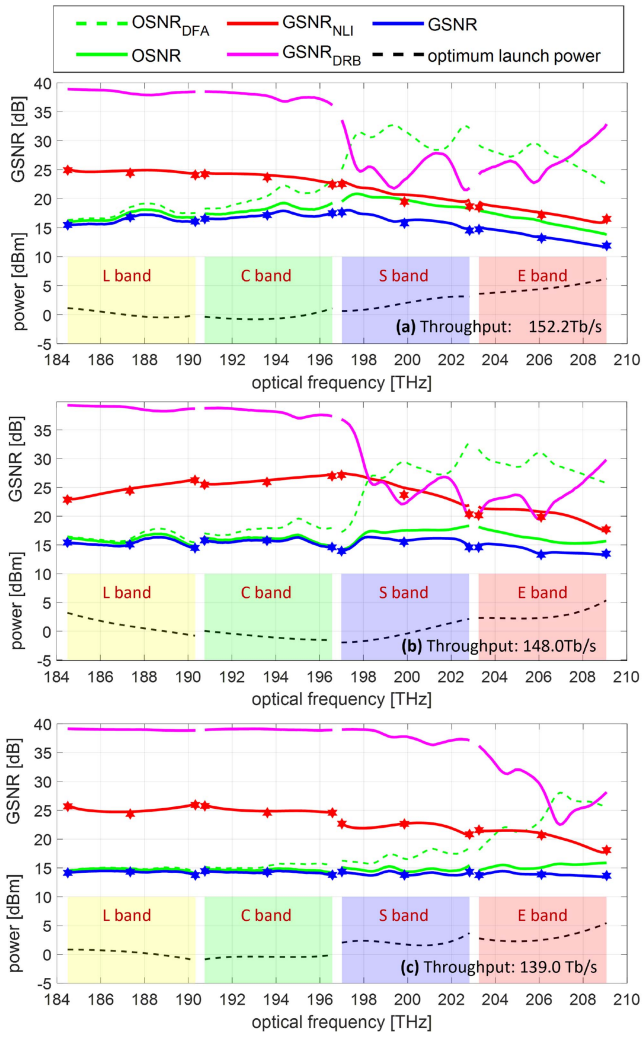

Fig. 7. CLSE optimum launch power per channel and GSNRs for (a) throughput maximization using (11); (b) throughput maximization while flattening GSNR using (12) with $w = 0.5$; (c) throughput maximization while flattening GSNR using (12) with $w = 1$.

from 124.6 Tb/s in Fig. 4(a). All BRPs were moved about 1 THz farther away from the signal, by the optimization, resulting in an improvement of the performance in the higher-S band, but they still provided some amplification to C band. The GSNR in the highest-frequency channel goes up to 15.5 dB, gaining 1.6 dB compared to Fig. 4(a).

To achieve an even flatter GSNR, w was set to 1 in Fig. 4(c). The optimum launch power per channel is represented by the dashed black curve, with average power of 1.1 dBm, 3.1 dBm and 2.8 dBm in the L, C and S band, respectively. The optimized BRPs are listed in Table I. The peak-to-peak GSNR variation was only 0.7 dB but the throughput experienced a bigger reduction, down to 113.7 Tb/s, about 10% lower than the value found when only maximizing throughput. Notice that now propagation is mostly linear with only about 1/3 of the C-band channels and 1/4 of the S-band channels in non-linear regime. All BRPs were moved farther away from the signal, by the optimization, to concentrate on S-band amplification, making the DRB noise negligible in both C and L bands.

We then looked at a CLSE system. The optimum launch power per channel is represented by the dashed black curve in Fig. 7. The optimized BRPs are listed in Table I. Maximum throughput optimization achieved 152.2 Tb/s, a 22.2% growth from CLS. The GSNR results are shown in Fig. 7(a) and SPPs plots are shown in Fig. 8. Note that about 1/2 of the channels are in non-linear regime, where DRB noise is also significant. We then again introduced GSNR flatness in the objective function, reducing GSNR variation from 6.2 dB to 3.0 dB with $w = 0.5$ in (b) and 0.8 dB with $w = 1$ in (c), at 148.0 Tb/s (b) and 139.0 Tb/s (c) throughput in Fig. 7. As BRPs went further away from the signal, more and more channels were in linearity, and DRB noise became negligible.

DRB noise should be carefully managed when backward Raman amplification is significant. The Raman on-off gain shown in Fig. 6 demonstrates that the threshold is approximately 20 dB.

Note that other optimization solutions can be found by changing the weight of GSNR flatness in the objective function, resulting in a different trade-offs between total throughput and GSNR flatness.

These case-studies were conceived to provide a demonstration of the effectiveness of the SPP algorithm in a very complex multiband long-haul environment. We think that overall they do provide interesting results related to multiband system design and optimization, but the key aspect is algorithm performance, which is dealt with below.

D. Performance of Algorithms

Fig. 8 provides a picture of the very diverse SPPs of the different channels in the CLSE system of Fig. 7(a), which

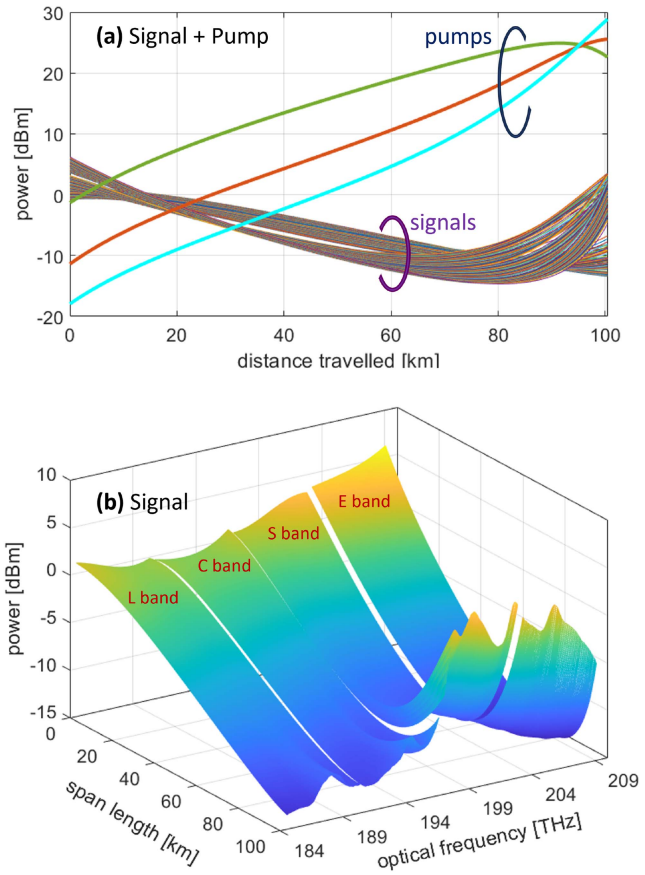

Fig. 8. SPPs in the first span (a) 2D plot of all lightwaves; (b) 3D plot of all signals in the CLSE system of Fig. 7(a).

constituted a very challenging scenarios for the SPP estimator, as well as the CFM6 and the optimizer algorithm itself.

To double check the accuracy of the CFM6 results, for some of the channels we ran the numerically-integrated full-fledged EGN model on the final optimized system configurations, obtaining the star markers shown in the figures. Comparing markers with solid lines, CFM6 shows very good accuracy, even in difficult high non-linearity situations, with heavy ISRS and strong backward Raman amplification. As expected, CFM6 turned out to be absolutely essential, since the optimizations shown above needed on average 2000 full system evalutions each, which would be very challenging to run with numerically integrated NLI models.

CFMs solve the NLI estimation problem but system optimization would not have been possible without the key boost provided by the SPP evaluation algorithm. It improved SPP computation speed by a factor of about 200 when compared to the reference dual-direction Raman solver (bvp4c in MATLAB). As for its accuracy, we looked at 1,030,000 channel and pump power values, sampled along the links at 100 m intervals, as found by the bvp4c algorithm and by our new SPP method. We found a max difference of $\pm$ 0.02 dB, proving the very good accuracy of the algorithm.

Regarding speed, one complete calculation of GSNR across 200 channels with CFM6, for the system of Fig. 7(a), took about 12 seconds. It is implemented in MATLAB(TM) and executed on a desktop PC equipped with a 12th Gen Intel(R) Core(TM) i9-12900 processor, operating at a clock speed of 2.40 GHz. We did not make use of any GPU support in the calculations. It was distributed as follows: SPP assessment and NLI evaluation with the CFM, 21% each; DRB estimation, 58.0%. Notably, DRB estimation appears to be the most time-consuming component. However, we made no attempt to speed up DRB estimation. We believe it has large margins of improvement and is not the focus of this paper.

In comparison, when using the conventional methods for SPPs calculation, one complete system performance calculation took 475 seconds, with 98.0% for SPPs, 0.5% for CFM and 1.5% for DRB assessment. This shows that the fast SPP algorithm grants a 40x speed improvement overall. If DRB noise was not taken into account, or was made considerably faster, the overall speed improvement would 100x. Regarding SPP evaluation alone, the speed up is a remarkable 200x.

IV. Conclusion

Fast full system performance estimation is essential for the deep iterative optimization of multiband systems. Its two time-consuming steps are NLI estimation and spatial power profile (SPP) computation for each channel and Raman pump. NLI estimation speed has been greatly reduced by fast closed-form GN/EGN models (CFMs). We have presented here a method that tackles the SPP estimation by substantially speeding it up, without losing accuracy. We have shown its potential by performing a C+L+S and a C+L+S+E 1000 km system optimization, with 3 Raman pumps. Overall, the system GSNR assessment was sped up by a factor of about 100. Thanks to such speed-up, deep optimization was possible,s system configurations were achieved with high overall system performance in test study-cases. For instance, a C+L+S+E system achieved a 4.5x throughput increase with respect to a super-C system, while also providing good GSNR flatness.

Appendix

A. Implementation of the SPP Algorithm in CLS System

The implementation and general algorithm description has been described with the pseudo-code in Section II. In this section, the CLS system with throughput maximization in Fig. 4(a) is used to demonstrate the implementation of the proposed algorithm. A few SPPs are reported in Fig. 9.

In this case study, the sum of the launch powers of the BRPs at $z = L_{\text{span}}$ is 7.5 dB ($t_{s,\text{dB}}$) higher than the sum of the launch powers of the transmission channels at $z = 0$.

If no modification is imposed on the BRPs, similar to [14], the initial SPPs are calculated based on the nominal launch powers of all lightwaves and the intrinsic fiber loss, which generates $[\mathbf{P}^{(0)}_{\text{signal}}; \tilde{\mathbf{P}}^{(0)}_{\text{pump}}]$ with $\tilde{\mathbf{P}}^{(0)}_{\text{pump}}$ shown as the dashed curves in Fig. 9(a). When using these SPPs as $\mathbf{P}^{(0)}$, the algorithm would diverge immediately (output all NaN in a few iterations) due to the significant power transfer from BRPs to signals at the fiber end.

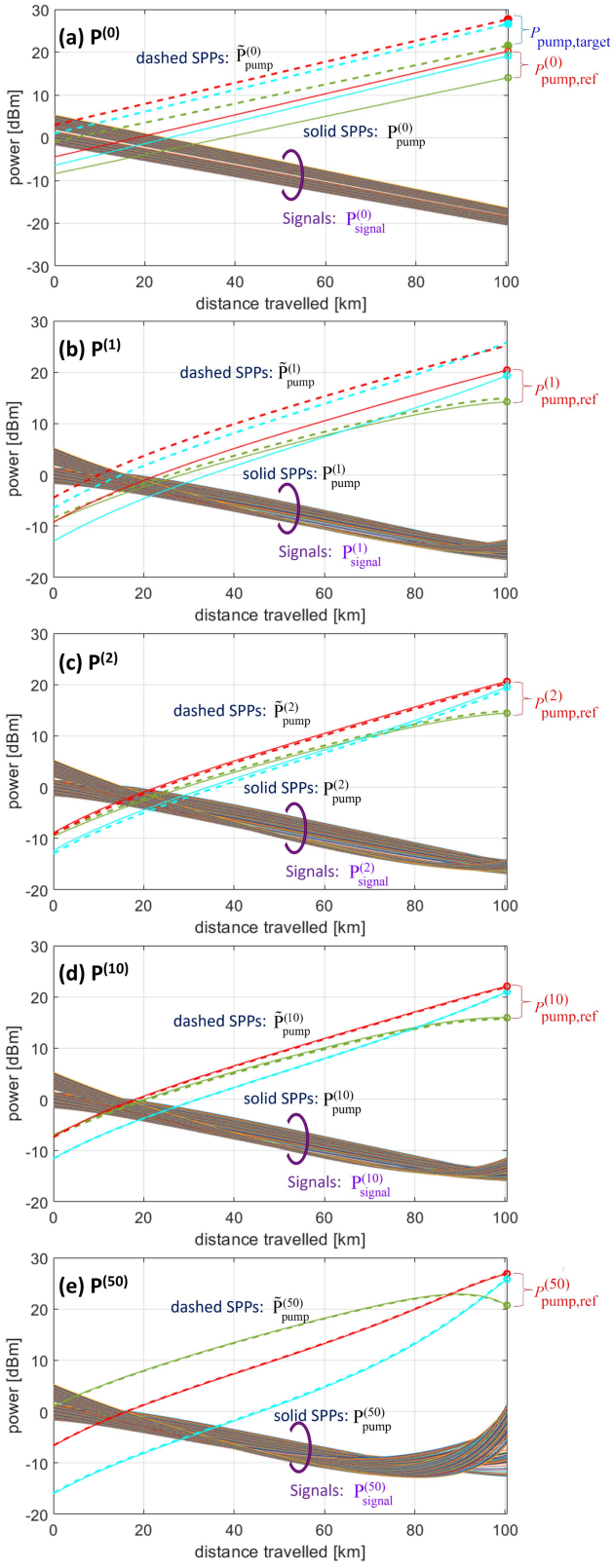

Fig. 9. SPPs evolution in CLS system with throuhgput maximization: (a) SPPs initialization $\mathbf{P}^{(0)}$ without considering ISRS. The three dots represent the nominal pump power; (b) SPPs $\mathbf{P}^{(1)}$ after the 1st iteration;(c) SPPs $\mathbf{P}^{(2)}$ after the 2nd iteration; (d) SPPs $\mathbf{P}^{(10)}$ after the 10th iteration; (e) SPPs $\mathbf{P}^{(50)}$ after the 50th iteration. After 75 iterations, SPPs converge to the solution in Fig. 5(a).

With the proposed initialization method, $\tilde{\mathbf{P}}^{(0)}_{\text{pump}}$ is pushed down of 7.5 dB to $\mathbf{P}^{(0)}_{\text{pump}}$ (the three solid curves) in Fig. 9(a), yielding a good initial SPPs $\mathbf{P}^{(0)} = [\mathbf{P}^{(0)}_{\text{signal}}; \mathbf{P}^{(0)}_{\text{pump}}]$.

We also define the number of iterations L_{iter} based on the law that 10 dB is recovered in 100 iterations, and obtain $L_{\text{iter}} = 75$. $\delta^{(k)}_{\text{dB}}$ is set as 0.2 dB at the first iteration, decreasing linearly to 0 dB at the last iteration.

Notably, $\delta^{(k)}_{\text{dB}}$ simultaneously defined BRPs powers reference $P^{(k)}_{\text{pump,ref}}$ for each iteration, as the circles shown in Fig. 9.

After the initialization, loading $\mathbf{P}^{(0)}$ into (3) generates $\tilde{\mathbf{P}}^{(1)} = [\mathbf{P}^{(1)}_{\text{signal}}; \tilde{\mathbf{P}}^{(1)}_{\text{pump}}]$ in the forward direction. As ISRS starts to count, $\tilde{\mathbf{P}}^{(1)}$ deviate significantly from $\mathbf{P}^{(0)}$. The signals gain some power from BRPs and start to bend up slightly. The BRPs powers at $z = L_{\text{span}}$ are completely off from $P^{(1)}_{\text{pump,ref}}$ as it is impossible to impose any constraint at $z = L_{\text{span}}$. We then rescale $\tilde{\mathbf{P}}^{(1)}_{\text{pump}}$ to match with $P^{(1)}_{\text{pump,ref}}$ at $z = L_{\text{span}}$ and obtain $\mathbf{P}^{(1)}$. This completes the first iteration of the algorithm. All SPPs are shown in Fig. 9(b).

Repeating the same procedure can generate $\mathbf{P}^{(2)}$ (Fig. 9(c)), and so on. Fig. 9 displays also $\mathbf{P}^{(10)}$ (Fig. 9(d)) and $\mathbf{P}^{(50)}$ (Fig. 9(e)), demonstrating a stable iteration towards the final solution. After 75 iterations, all BRPs get back to the launch powers and the algorithm stops. Generally, the last ten $\delta^{(k)}_{\text{dB}}$ are quite small for fine-tuning the solution.

If the algorithm can not deal with the problem, it would diverge within a few iterations, and all SPPs values would accumulate quickly to NaN. We then move to the conventional method. However, this did not happen in all the study cases.

REFERENCES

[1] Y. Jiang et al., "Optimization of long-haul CLS systems by means of a closed form EGN model," *Photon. Technol. Lett.*, vol. 36, no. 18, pp. 1129–1132, Sep. 2024.

[2] B. J. Puttnam et al., "339.1 Tb/s OESCLU-band transmission over 100 km SMF," presented at the Eur. Conf. Opt. Commun., Frankfurt, Germany, Sep. 22–26, 2024, pp. 43–46.

[3] I. Kim et al., "Band-wise Bidirectional S+C+L transmission in hybrid Raman-EDFA link," presented at the Eur. Conf. Opt. Commun., Frankfurt, Germany, Sep. 22–26, 2024, pp. 59–62.

[4] B. J. Puttnam et al., "High data-rate OESCLU-Band transmission," *J. Lightw. Technol.*, early access, Feb. 18, 2025. doi: 10.1109/JLT.2025.3543448.

[5] S. Shimizu et al., "27-THz ISRS-supported transmission over 1040 km in S+C+L+U and extreme longer-wavelength band," presented at the Opt. Fiber Commun. Conf., Los Angeles, CA, USA, Mar. 30–Apr. 03, 2025, Paper Th4A.2.

[6] P. Poggiolini, G. Bosco, A. Carena, V. Curri, Y. Jiang, and F. Forghieri., "The GN-Model of fiber non-linear propagation and its applications," *J. Lightw. Technol.*, vol. 32, no. 4, pp. 694–721, Feb. 2014.

[7] A. Carena, G. Bosco, V. Curri, Y. Jiang, P. Poggiolini, and F. Forghieri., "EGN model of non-linear fiber propagation," *Opt. Exp.*, vol. 22, no. 13, pp. 16335–16362, 2014.

[8] H. Buglia et al., "A closed-form expression for the Gaussian noise model in the presence of inter-channel stimulated Raman scattering extended for arbitrary loss and fibre length," *J. Lightw. Technol.*, vol. 41, no. 11, pp. 3577–3586, Jun. 2023.

[9] H. Buglia et al., "A closed-form expression for the Gaussian Noise Model in the presence of Raman Amplification," *J. Lightw. Technol.*, vol. 42, no. 2, pp. 636–648, Jan. 2024.

[10] P. Poggiolini and M. Ranjbar-Zefreh, "Closed form expressions of the nonlinear interference for UWB systems," presented at the Eur. Conf. Exhib. Opt. Commun., Basel, Switzerland, Sep. 18–22, 2022, pp. 1–4.

[11] Y. Jiang et al., "Closed-form EGN model with comprehensive Raman support," presented at the Eur. Conf. Opt. Commun., Frankfurt, Germany, Sep. 22–26, 2024, pp. 1431–1434.
[12] V. E. Perlin and H. G. Winful, "Optimizing the noise performance of broad-band WDM systems with distributed raman amplification," *Photon. Technol. Lett.*, vol. 14, no. 8, pp. 1199–1201, Aug. 2002.
[13] K. Kimura, S. Shimizu, T. Kobayashi, M. Nakamura, and Y. Miyamoto, "Accurate SNR estimation in C+L-band 10-THz hybrid Raman-EDFA amplified transmission using two-stage power profile calculation accounting for pump depletion," presented at the Opt. Fiber Commun. Conf., San Diego, CA, USA, Mar. 24–28, 2024, Paper M1F.5.
[14] L. K. Choi, P. Kim, J. Park, J. Park, and N. Park, "Adiabatic, closed-form approach to the highly efficient analysis of a fiber Raman amplifier problem," *Opt. Lett.*, vol. 30, no. 2, pp. 126–128, 2005.
[15] J. Sarkis, Y. Jiang, S. Piciaccia, F. Forghieri, and P. Poggiolini, "Signal and Raman pump launch power optimization in a CLSE system using fast power profile estimation," presented at the Opt. Fiber Commun. Conf., San Francisco, CA, USA, Mar. 30–Apr. 03, 2011, Paper Tu3K.3.
[16] J. Sarkis et al., "An algorithm to speed up the spatial power profile calculation in backward Raman amplified systems," 2024, *arXiv:2411.12688*.
[17] Y. Jiang et al., "Experimental test of a closed-form EGN model over C+L bands," *J. Lightw. Technol.*, vol. 43, no. 2, pp. 439–449, Jan. 2025.
[18] S. Walker, "Rapid modeling and estimation of total spectral loss in optical fibers," *J. Lightw. Technol.*, vol. 4, no. 8, pp. 1125–1131, Aug. 1986.
[19] K. Rottwitt, J. Bromage, A. J. Stentz, Lufeng Leng, M. E. Lines, and H. Smith., "Scaling of the Raman gain coefficient: Applications to Germanosilicate fibers," *J. Lightw. Technol.*, vol. 21, no. 7, pp. 1652–1662, Jul. 2003.
[20] C. Dibon et al., "Experimental validation of DRS impact on transmission systems at 2.5, 10 and 40Gbit/s," presented at the Eur. Conf. Opt. Commun., Copenhagen, Denmark, Sep. 8–12, 2002, pp. 1–2.
[21] V. E. Perlin and H. G. Winful, "On trade-off between noise and nonlinearity in WDM systems with distributed raman amplification," in *Proc. Opt. Fiber Commun. Conf. Exhibit*, Anaheim, CA, USA, 2002, pp. 178–180.
[22] M. R. Zefreh, F. Forghieri, S. Piciaccia, and P. Poggiolini, "Accurate closed-form real-time EGN model formula leveraging machine-learning over 8500 thoroughly randomized full C-band systems," *J. Lightw. Technol.*, vol. 38, no. 18, pp. 4987–4999, Sep. 2020.
[23] G. Bosco et al., "Performance prediction for WDM PM-QPSK transmission over un-compensated links," presented at the Opt. Fiber Commun. Conf., Los Angeles, CA, USA, Mar. 6–10, 2011, pp. 1–3.